ISSN 2231-5063 Impact Factor : 4.6052 (UIF) Volume - 6 | Issue - 2 | August - 2016

Golden Research Thoughts

ANALYSIS OF DIFFERENT FIELD WORKS

Anand Mohan
Research Scholar , L.N.M.U Darbhanga .

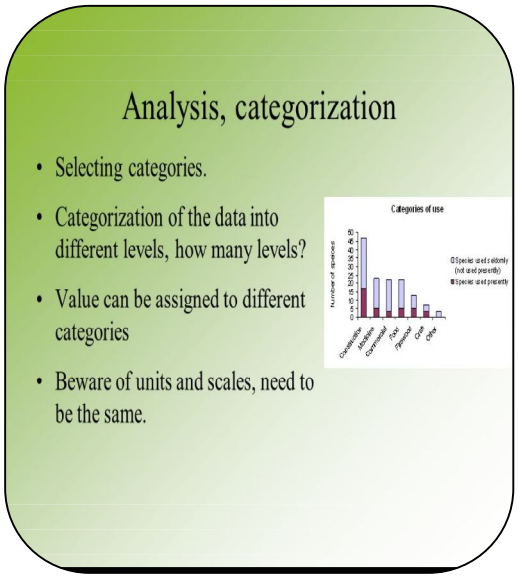

2.1. THE INDUCTION COIL FIELD:

The induction or search coil, which is one of the simplest magnetic field sensing devices, is based on Faraday's law. This law states that if a loop of wire is subjected to a changing magnetic flux, through the area enclosed by the loop, then a voltage will be induced in the loop that is proportional to the rate of change of the flux:

$$e(t) = -\frac{d\phi}{dt} \quad \text{----------2.1}$$

Induction or search coil sensors consist of a loop of wire (or a solenoid), which may or may not surround a ferromagnetic core. (a) Air core loop antenna; (b) solenoid induction coil antenna with ferromagnetic core. Since magnetic induction *B* is flux density, and then a loop with cross-sectional area *A* will have a terminal voltage:

$$e(t) = -\frac{d(\bar{B} \bullet \bar{A})}{dt} \quad \text{----------2.2}$$

Equation 2.2 states that a temporal change in $\overline{B}$ or the mechanical orientation of $\overline{A}$ will produce a terminal voltage. If the coil remains fixed with respect to $\overline{B}$, then static fields cannot be detected; but if the loop is rotated or the magnitude of $\overline{A}$ is changed, then it is possible to measure a static field. The relationship described by Equation 2.2 is exploited in many magnetic field measuring instruments. Figure 2.2 shows the most common induction coil configurations for measuring field strength of the air core loop antenna and the rod antenna.

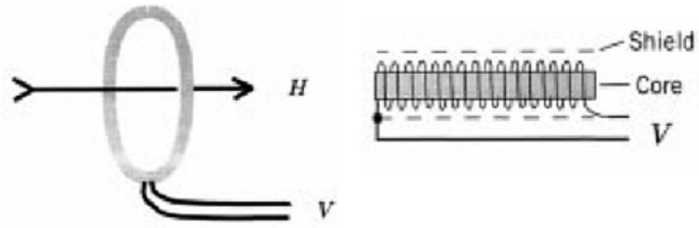

Figure 2.2

The operating principle is the same for both configurations. Substituting $\mu_0 \mu_e H(t)$ for *B* in Equation 2.2 and, assuming the loop is stationary with respect to the field vector, the terminal voltage becomes:

$$e(t) = -\mu_0 \mu_e nA \frac{dH(t)}{dt} \quad \text{----------2.3}$$

Where *n* is the number of turns in the coil, and μ is the effective relative permeability of the core. The core of a rod antenna is normally constructed of magnetically "soft" material so one can assume the flux density in the core is induced by an external magnetic field and, therefore, the substitution above is valid. With an air core, the effective relative permeability is one.

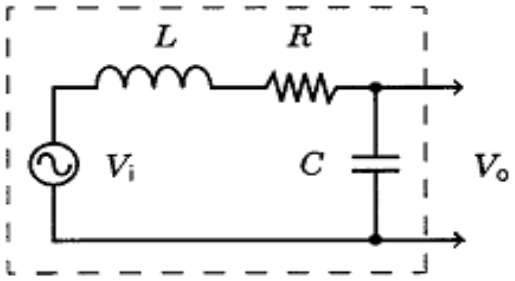

Figure 2.3 The induction coil equivalent circuit is a frequency-dependent voltage source in series with an inductor, resistor, and lumped capacitor.

The effective permeability of an induction coil that contains a core is usually much greater than one and is strongly dependent on the shape of the core and, to some extent, on the configuration of the winding. Taking the Laplace transform of Equation 2.3 and dividing both sides by *H,* one obtains the following transfer function *T*(*s*) for an induction coil antenna:

$$T(s) = -\mu_0 \mu_e nAs = -Ks \quad \left(\mathrm{VmA^{-1}}\right) \text{----------1.4}$$

Where *E*(*s*) = *T*(*s*) *H*(*s*), *E*(*s*) and *H*(*s*) are the Laplace transforms of *e*(*t*) and *H*(*t*), and *s* is the Laplace transform operator. Inspection of Equation 2.3 reveals that the magnitude of the coil voltage is proportional to both the magnitude and frequency of the magnetic field being measured. The coil constant or sensitivity of the loop antenna is:

$$K = \mu_0 \mu_e nA \quad \left(\mathrm{VsmA^{-1}}\right) \text{----------2.5}$$

Figure 2.3 is the equivalent circuit for an induction coil antenna. The actual voltage measured at the terminals of the loop is modified by the inductance *L*, resistance *R*, and the distributed stray and shield capacitances represented by the lumped capacitor *C*. These circuit parameters depend on the geometry of the core, coil, and winding. The electrostatic shield made of nonmagnetic material shown in Figure 2.3 is an important element in the design of an induction coil. It prevents coupling of electric fields into the coil, thereby assuring that the signal seen at the coil terminals is only that due to a magnetic field. The shield should not be placed too close to the winding since it contributes to coil capacitance and noise.

2.2. THE AIR CORE LOOP FIELD:

The air core loop antenna consists of a circular or rectangular loop containing one or more turns of wire and no magnetic core. The diameter of the loop is usually much greater than the dimensions of the winding cross-section. The sensitivity of a circular loop antenna with a winding inside diameter *d* and rectangular cross-section is approximately:

$$K = \mu_0 n\pi \frac{d^2}{4}\left[1 + 2\left(\frac{t}{d}\right) + \frac{3}{4}\left(\frac{t}{d}\right)^2\right. \text{----------2.6}$$

Where *t* is the thickness of the winding and *n* is the number of turns. The resistance of the coil is:

$$R = 4n\frac{d}{d_w^2}\left(1 + \frac{t}{d}\right)\rho\ \Omega \text{----------2.7}$$

Where d_w is the diameter of the bare wire and ρ is its resistivity in Ω m (1.7 × 10 Ω m for copper) [5]. The inductance of the coil is more difficult to compute since it depends heavily on the geometry of the coil. Equation 2.8 is a general expression that gives a good approximation for the inductance of a circular air core coil.

$$L = \mu_0 n^2 \pi \left(\frac{\bar{d}}{2}\right)^2 \frac{k}{w} \text{ H} \quad \text{----------2.8}$$

Where *w* is the width of the winding, *d* is the average diameter, and *k* is Nagaoka's constant:

$$k = \frac{1}{1 + 0.45\frac{\bar{d}}{w} + 0.64\frac{t}{\bar{d}} + 0.84\frac{t}{w}} \quad \text{----------2.9}$$

The distributed capacitance of the coil contributes the most to the overall antenna capacitance. The parasitic capacitances can usually be ignored. Equation 2.10 can be used to estimate the distributed capacitance of a coil.

$$C_d = \left[\frac{\varepsilon_w \varepsilon_l}{\varepsilon_w t_l + \varepsilon_l t_w}\right] \frac{0.018544\,\bar{d} w (n_l - 1)}{n_l^2} \quad \text{---------- 2.10}$$

where ε_w is the dielectric constant of the wire insulation, ε is the dielectric constant of the interlayer insulation if any, t_w is the thickness of the wire insulation, t_l is the thickness of the interlayer insulation, and *n* is the number of layers. Adding a second layer to a single-layer coil significantly increases the capacitance but, as the number of layers increases, the capacitance decreases. The air core loop antenna is particularly useful for measuring magnetic fields with frequencies from 100 Hz to several megahertz. Because it has a linear response to magnetic field strength, it has virtually no intermodulation distortion. On the negative side, the size of the sensor can get quite large for applications that require high sensitivities at low frequencies. The rod antenna is a good alternative to an air core loop antenna. It is smaller in size than a loop antenna with the same sensitivity, and it can be designed to operate at lower frequencies. Unfortunately, its response to magnetic field strength can be nonlinear and the core adds noise. Figure 2.2(b) is a typical configuration for a rod antenna. It is basically a solenoid with a magnetic core. The core can have a circular or rectangular cross-section and can be made from a ferrite, a nickel iron alloy, an amorphous metal glass alloy, or some other material with high relative permeability. The winding can be wound directly on the core or on a form through which the core is inserted. Insulation is sometimes placed between layers of the winding to reduce distributed capacitance. An electrostatic shield is placed around the winding to attenuate any electric field coupling into the signal. The shield has a gap that runs the length of the winding. This prevents circulating currents in the shield from attenuating the magnetic field within the coil. The most common rod antenna configuration is a core with a circular cross-section and a tightly coupled winding that runs most of the length of the core. The sensitivity of the rod antenna is computed by substituting μe in Equation 2.11 with the following:

$$\mu_e = 1 + \left(\frac{d_c}{d+t}\right)^2 (\bar{\mu} - 1) \quad \text{---------- 2.11}$$

Where d_c is the core diameter and $\bar{\mu}$ is the core average effective permeability. The core effective or apparent permeability depends on its geometry and initial permeability, as well as the winding length relative to the core length. A rod becomes magnetized when a magnetic field is applied to it. In response, a magnetic field is created within the rod that opposes the externally applied field and reduces the flux density. The demagnetizing field is proportional to the magnetization and the net field *H* in the core is:

$$H = H' - NM \quad \text{----------2.12}$$

Where *H'* is the applied external field, *N* is the demagnetizing factor, and *M* is the magnetization. The apparent relative permeability of a core is the ratio of the flux density *B* in the middle of the core to the flux density in air:

$$\frac{B}{\mu_0 H'} = \mu_a = \frac{\mu_l}{1 + N(\mu_l - 1)} \quad \text{---------- 2.13}$$

Where μ_l is the initial relative permeability of the core material. Initial relative permeability is the slope of the *B–H* magnetization curve near zero applied field for a closed magnetic path. The value of *N* is shape dependent. As the

length-to-diameter ratio *m* of a rod increases, *N* decreases and the apparent relative permeability approaches the initial permeability. To be useful, the induction coil signal must be conditioned using either a voltage or a current amplifier. Figure 2.4 illustrates the circuit configurations for both of these signal conditioning methods. The voltage amplifier can have either a single-ended or differential input and it can be tuned or un tuned.

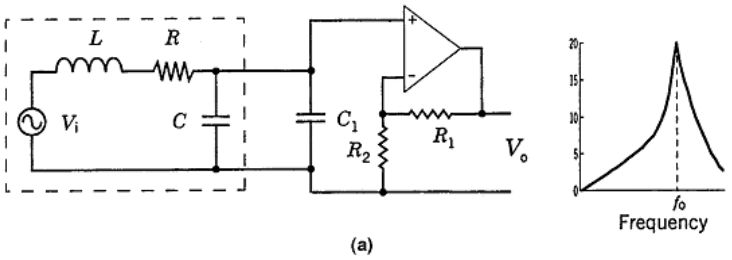

Figure 2.4. (a)The amplitude of a voltage amplified induction coil signal is proportional to the frequency and strength of the field

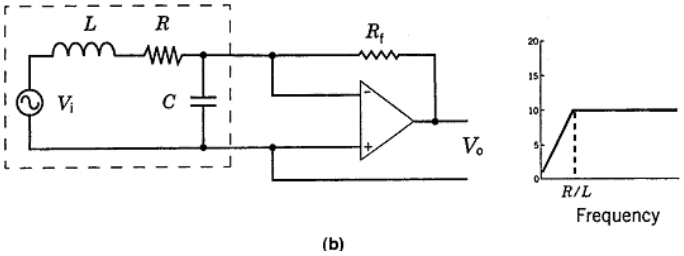

Figure 2.4. (b) The amplitude of a current amplified induction coil signal is proportional to field strength beyond its L/R corner frequency.

The signal output of the voltage amplifier is proportional to the magnitude and frequency of the field for frequencies well below resonance. Its output will peak at the resonant frequency of the coil or at the tuning frequency. Because its output signal depends on both the frequency and strength of the magnetic field, the voltage amplifier is more suited to narrow band or tuned frequency applications.

In the current amplifier configuration, the induction coil terminals are connected to a virtual ground. As long as the product of the amplifier forward gain and the coil ohmic resistance is much greater than the feedback resistor, the output signal magnitude is independent of the frequency of the magnetic field beyond the *R*/*L* (rad s) corner of the coil. This remains true up to the coil's resonant frequency. For this reason, the current amplifier configuration is particularly suited to broadband magnetic field strength measurements. The current amplifier configuration minimizes intermodulation distortion in induction coils with magnetic cores. The current flowing through the coil produces a magnetic field that opposes the ambient field. This keeps the net field in the core near zero and in a linear region of the *B*–*H* curve. Current-amplifier-based induction coil magnetometers have been built that have a flat frequency response from 10 Hz to over 200 kHz. Some magnetometers designed for geophysical exploration applications have low frequency corners that extend down to 0.1 Hz.

2.3 THE OPTICALLY PUMPED FIELD:

The optically pumped field is based on the Zeeman Effect. This effect is most pronounced in alkaline vapors such as rubidium, lithium, cesium, sodium, and potassium. Figure 2.4 is the hyperfine spectral structure for the valence electrons of rubidium (Rb) 85, which is commonly used in these types of magnetometers. The energy-related frequency interval between these hyperfine lines is proportional to the applied field. The magnetic quantum number *m* is related to the angular momentum number and specifies the possible component magnitude of the magnetic moment along the applied field. The optically pumped magnetometer takes advantage of this characteristic. Transitions occur between levels of different *m* values and obey the rule that the change in *m* can only have the values 0, 1, and –1. When not optically excited, the energy states of the valence electrons will be distributed according to Boltzmann statistics and will be in a state of equilibrium. If the electrons are excited with circularly polarized light at the D1 frequency (794.8 nm wavelength), they will absorb photons and transition takes place from the $^2S_{1/2}$ state to the $^2P_{1/2}$ state according to the

transition rules. The excited electrons will then fall back in a random fashion to the lower states, being distributed with an equal probability among all the *m* states. But the rules state that the change in *m* can only be 1 or –1 for polarized light. If one uses right circularly polarized light, then the change in *m* can only be 1, and the electrons in the *m* = 3 level of the $^2S_{1/2}$ state cannot transition since there is no *m* = 4 level at the 2P state. Therefore, these electrons remain in the *m* = 3 state. All other electrons transition to the higher state and then fall back to the lower state

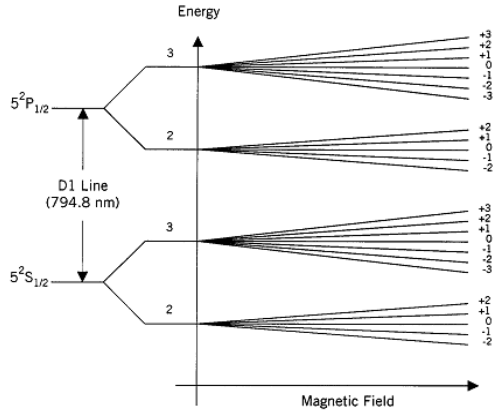

Figure 2.5 Rb-85 Energy diagram. When a magnetic field is applied, the energy levels split into Zeeman sublevels that diverge as the field increases. Quantum mechanical factors determine the number of sublevels at each primary energy level.

As a result, the sample rate and resolution can be much higher. A resolution of 0.005 nT is possible. Sampling rates can be as high as 15 samples per second. Descriptions of several optically pumped magnetometers and their operating principles can be found in. There are a number of different signal conditioning arrangements that can be used to derive a useful readout of the measured fields.

2.4. THE HALL FIELD:

The Hall Effect device, which is probably the most familiar and widely used sensor for measuring strong magnetic fields, is based on the discovery of the Hall Effect by Edwin H. Hall in 1897. The Hall effect is a consequence of the Lorentz force law, which states that a moving charge *q*, when acted upon by a magnetic induction field *B*, will experience a force *F* that is at right angles to the field vector and the velocity vector *v* of the charge as expressed by the following equation:

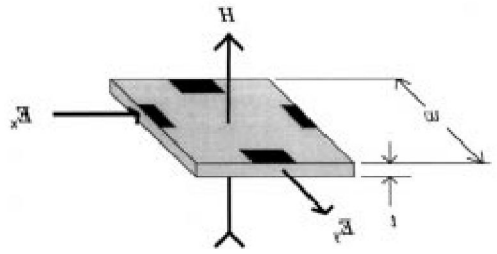

Figure 2.6 Hall -Effect sensor. A magnetic field *H* applied normal to the surface of the sensor, which is conducting current along the *x*-direction, will generate a voltage along the *y*-direction. *E* is the applied electric field along the *x*-direction, and *E*y is the Hall- effect electric field along the *y*-direction.

$$\vec{F} = -q\left(\vec{E} + \vec{v} \times \vec{B}\right) \quad \text{---------- 2.14}$$

The Hall Effect device consists of a flat, thin rectangular conductor or semiconductor with two pairs of electrodes at right angles to one another. An electric field *E* is applied along the *x* or control axis. When a magnetic field *B* is applied perpendicular to the surface of the device, the free charge, which is flowing along the *x*-axis as a result of *Ez*, will be deflected toward the *y* or Hall voltage axis. Since current cannot flow in the *y*-axis under open-loop

conditions, this will cause a buildup of charge along the *y*-axis that will create an electric field which produces a force opposing the motion of the charge:

$$J_X = qnv_x \quad \text{---------- 2.15}$$

$$E_y = \frac{jx\,Bz}{qn} = R_H J_X B_Z \quad \text{---------- 2.16}$$

Where *R* is called the Hall coefficient. A semiconductor is treated in terms of the mobility v (drift velocity/field) of the majority carrier H(electron or hole) and conductivity σ. In this case,

$$E_y = \mu E_x B_z \text{ and } E_x = \frac{J_x}{\sigma} \quad \text{---------- 2.17}$$

$$E_y = \frac{\mu}{\sigma} J_x B_z \text{ and } R_H = \frac{\mu}{\sigma} \quad \text{---------- 2.18}$$

The value of *R* varies substantially from one material to another and is both temperature and field magnitude dependent. Its characteristics can be controlled to a certain extent by doping the base material with some impurities. For example, doping germanium with arsenic can reduce the temperature dependence at the expense of magnitude. The voltage measured across the *y*-axis terminals is the integral of the electric field along the *y*-axis. If a constant control current *I* is flowing along the *x* axis, then:

$$J_x = \frac{I}{wt} \quad \text{----------2.19}$$

$$e_y = \frac{R_H I B_z}{t} \quad \text{----------2.20}$$

Where *t* is thickness (m) and *w* is the distance between the *y*-axis terminals. Another characteristic specified by manufacturers of Hall Effect devices is the magnetic sensitivity at the rated control current *I*c:

$$\gamma_b = \frac{e_y}{B_z} = \frac{R_H I_c}{t} \quad \text{----------2.21}$$

Although conductors such as copper (Cu) can be used to make a Hall effect device, semiconductor materials, such as gallium arsenide (GaAs), indium antimonide (InSb), and indium arsenide (InAs), produce the highest and most stable Hall coefficients. InAs, because of its combined low temperature coefficient of sensitivity (<0.1%/°C), low resistance, and relatively good sensitivity, is the material favored by commercial manufacturers of Hall Effect devices. The typical control current for Hall Effect devices is 100 mA, but we can also operate at currents as low as 1 mA. Linearity ranges from ¼% to 2% over their rated operating field range. The sensor element is usually tiny (on the order of 10 mm square by 0.5 mm thick), and a three-axis version can be housed in a very small package. These devices are most effective for measuring flux densities ranging from 50 T to 30 T.The Hall voltage can be conditioned and amplified by any high input impedance (>1 kohm) differential amplifier. A precision instrumentation amplifier is a good choice because it has adequate input impedance, its gain can be determined by a stable resistor, and the amplifier zero offset trim resistors can be used to cancel the zero offset of the Hall Effect device. Some devices require a load resistor across the Hall voltage terminal to achieve optimum linearity. The zero offset and 1/*f* noise of the Hall voltage amplifier limit the performance of a Hall Effect gauss meter for low field strength measurements.

2.5. ELECTRIC FIELD INSIDE A MATERIAL:

Electric field integral equation methods have been developed to quantify the induced electric field inside a material sample placed in an energized cavity. It was demonstrated that the integral equation method is a powerful technique because it can handle the material sample of arbitrary shapes and heterogeneities. The only disadvantage of this method is its slow numerical convergence and a large computation time. To provide a numerical check for the integral equation method, a mode-matching method is developed to study the same subject. We consider a cylindrical cavity coaxially loaded with a homogeneous material sample of simple geometry and excited by a current probe. A mode-matching method combined with a Green's function technique for the excitation probe is applied to determine the induced electric field inside the material sample as well as the fields in other parts of the cavity. Analytical results of

the mode-matching method are then used to verify the numerical accuracy of the integral equation method. It is noted that the mode-matching method can only handle homogeneous material samples with simple geometries. However, it can provide sufficient information for the verification of the integral equation method. In fact, the mode-matching method has been used by a number of workers to analyze dielectric-loaded cavities. These previous studies were mainly concerned with the resonant frequency and the field distribution, and the excitation of a current probe was not considered. Similar problems involving the interaction of the cavity field and a material sample inside a cavity have been studied by other methods, including the surface integral equation method, the finite difference time domain method, the finite element method and the method of lines. Applying the mode-matching method to a homogeneous material sample with a simple cylindrical geometry placed within a cylindrical cavity, we can divide the cavity into three waveguide regions as shown in Fig. 2.6, where regions I and III are the normal waveguide regions filled with a homogeneous material or empty and region II is the in homogeneously filled waveguide region containing the material sample. The waveguide Eigen modes in region II are derived first while those in regions I and III are well known. The EM fields in each region are expressed in terms of its Eigen modes, and the tangential components of the electric and magnetic fields are matched at the junctions of the three regions. The equations resulted from the matching of the boundary conditions are then numerically solved. The numerical results agree well with that obtained using the integral equation method. It is also shown that the mode-matching method can save a great deal of computation time attributed to the use of the well-defined Eigen modes and sparse resultant matrices.

2.6. ANALYSIS OF THE INDUCED ELECTRIC FIELD:

The geometry of an in homogeneously filled waveguide is shown in Fig. 2.7 which consists of two sub-regions having the same central axis. The central sub-region is a homogeneous material sample and the outer sub-region is empty space.

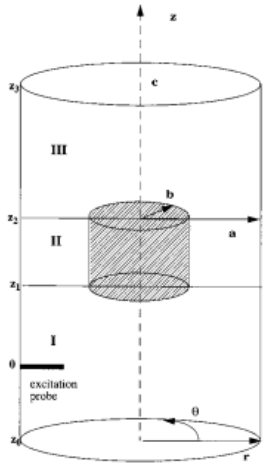

Figure 2.7. Geometry of the material sample placed in a cylindrical cavity driven by an excitation probe.

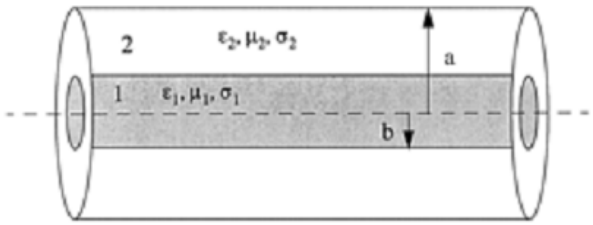

Figure 2.8. Geometry of the in homogeneously filled waveguide which is region II in Fig. 1.7.

We have dealt with the homogeneous material samples with simple cylindrical geometries which have been placed coaxially in the cavity. The normal Eigen modes in this in homogeneously filled waveguide are not, in general, either TE or TM modes, but a combination of an TE and an TM mode, a hybrid Eigen mode. In Fig. 2.8, the dielectric parameters of sub-region 1 are: relative permittivity ε_1, permeability $\mu_1$and conductivity σ_1, and its radius b. The parameters of sub-region 2 are: relative permittivity ε_2 , permeability $\mu_{2\ and}$ conductivity σ_2 with radius a. Based on the

relations between the longitudinal and the transverse components of the electromagnetic fields, we obtain the electromagnetic Eigen modes in these two sub-regions .we can numerically obtain the propagation constant for each Eigen mode and then determine the corresponding eigenvalues k and thus, the Eigen modes in this in homogeneously filled waveguide can be determined. The electromagnetic fields in each region can then be expressed as the infinite summations of the Eigen modes in the corresponding region.

REFERENCES

[1] Aboaf, J. A., Herd, S. R. & Klokholm, E. Magnetic properties and structure of cobalt platinum thin films. IEEE Trans. Magn. 19, 1514–1519 (1983)

[2]. B. Chu, X. Zhou, K. Ren, B. Neese, M. Lin, Q. Wang, F. Bauer and Q. M. Zhang, Science 313, 334 (2006).

[3]. Bernand-Mantel, A. et al. Electric-field control of domain wall nucleation and pinning in a metallic ferromagnet. Appl. Phys. Lett. 102, 122406 (2013).

[4] Bauer, U., Emori, S. & Beach, G. S. D. Voltage-controlled domain wall traps in ferromagnetic nanowires. Nature Nanotech. 8, 411-416 (2013).

[5] Boulle, O., Malinowski, G. & Kläui, M. Current-induced domain wall motion in nanoscale ferromagnetic elements. Mat. Sci. Eng. R 72, 159–187 (2011).

[6]. Baure ´ us, C.L.M., Sommarin, M., Persson, R.R.R., Salford, L.G., and Eberhardt, J.L. (2003). Interaction between weak low frequency magnetic fields and cell membranes. Bioelectromagnetics 24, 395.

[7]. Belova, N.A., and Lednev, V.V. (2000). Dependence of the gravitropic response in flax stem segments on the frequency and amplitude of a weak combined magnetic field. Biophysics 1075, 45, 1108.